Chapter 10

Observation and Modeling of Net Ecosystem Carbon Exchange Over Canopy

Tomo'omi Kumagai*
Institute for Space-Earth Environmental, Nagoya University, Chikusa-ku, Nagoya 464-8601, Japan

Summary

Eddy covariance, which is the most common micrometeorological flux measurement method, can estimate ecosystem-scale and fine time-resolution carbon dioxide (CO_2) exchange between the upper vegetation surface and atmosphere. Given no lateral CO_2 advection, the sum of eddy covariance measurements and CO_2 storage in the underlying air represents net ecosystem-atmosphere CO_2 exchange (N_E). Although observation, analysis and prediction of N_E are major concerns in terms of terrestrial ecosystem carbon balance, there are many difficulties in obtaining reasonable observation values. N_E observation is based on fluid dynamics principles and turbulence theory; thus, model computations to reproduce N_E observation should reflect the theory for N_E mechanisms and processes. The Soil-Vegetation-Atmosphere Transfer (SVAT) model is a promising tool for validation of magnitude and analysis of N_E formation.

Keywords Energy, H_2O, and CO_2 exchange between land and atmosphere • Eddy covariance measurement • Flux observation • Boundary layer meteorology

*Author for correspondence, e-mail: tomoomikumagai@gmail.com

K. Hikosaka, Ü. Niinemets, and N.P.R. Anten (eds.), *Canopy Photosynthesis: From Basics to Applications*, DOI 10.1007/978-94-017-7291-4_10

I. Introduction

Energy and materials exchange between the vegetation canopy and atmosphere can be directly measured using the basics of fluid dynamics, called micrometeorological methods (Moncrieff et al. 2000). In general, the micrometeorological flux measurement methods are conducted with installation of automatic and frequent-sampling sensors above the canopy. These report temporal flux variations at intervals of several tens of minutes and integrate the fluxes over horizontal length scales between 100 m and several kilometers.

Eddy covariance typically provides a direct and sequential estimate of carbon dioxide (CO_2) flux absorbed/released by the vegetation canopy from/to the atmosphere with fine temporal resolution. The CO_2 flux referred to here denotes exchange between the canopy and atmosphere resulting from the integration of CO_2 absorption (leaf photosynthesis) and evolution (leaf, branch, stem and root respiration, and soil organic matter decomposition) within the canopy (Fig. 10.1). Reliable and reasonable flux

Abbreviations: ABL – Atmospheric boundary layer; A_l – Leaf photosynthesis rate; $A_{lsh} - A_l$ for shaded leaves; $A_{lsl} - A_l$ for sunlit leaves; a_{leaf} – Leaf area density; a_{sh} – Shaded leaf area density; a_{sl} – Sunlit leaf area density; ASL – Atmospheric surface layer; b_L – Intercept of the stomatal conductance model (Ball et al. 1987; Collatz et al. 1991); c – CO_2 concentration in the air; CBL – Convective boundary layer; C_d – Drag coefficient; C_i – CO_2 concentration within the stomatal cavity; c_p – Specific heat of air at constant pressure; C_s – CO_2 concentration of air inside the laminar boundary layer of leaves; CSL – Canopy sub-layer; e – Atmospheric water vapor pressure; E_l – Water vapor flux per unit of leaf area; $E_{lsh} - E_l$ for shaded leaves; $E_{lsh} - E_l$ for sunlit leaves; $e_{sat}(T_l)$ – Saturation vapor pressure at leaf temperature (T_l); e_{tk} – Turbulent kinetic energy; F_A – CO_2 flux without soil respiration; F_c – Vertical CO_2 flux; FLUXNET – Global network of flux tower sites; g_{ac} – Boundary conductance for CO_2; g_{ah} – Boundary conductance for heat; g_{aw} – Boundary layer conductance for water vapor; g_{sc} – Stomatal conductance for CO_2; g_{sw} – Stomatal conductance for water vapor; GSWP – Global Soil Wetness Project; g_w – Total conductance for water vapor; h_c – Forest canopy height; H_l – Sensible heat flux per unit of leaf area; $H_{lsh} - H_l$ for shaded leaves; $H_{lsh} - H_l$ for sunlit leaves; h_s – Relative humidity of air inside the boundary layer of a leaf; H_{soil} – Sensible heat flux at the soil surface; J_C – Ribulose bisphosphate (RuBP) carboxylase/oxygenase activity; J_E – Rate of RuBP regeneration through electron transport; J_{max} – Potential rate of whole-chain electron transport; $J_{max\_25} - J_{max}$ at 25 °C; J_S – Export rate of synthesized sucrose; K_t – Eddy turbulent diffusivity; L – Long-wave radiation at the given height; LAI – Leaf area index; LE – Latent heat flux; LT – Local time; m_a – Molecular weight of air; m_e – Molecular weight of water; m_L – Slope of the stomatal conductance model (Ball et al. 1987; Collatz et al. 1991); NCEP-NCAR – National Centers for Environmental Prediction – National Center for Atmospheric Research; N_a – Leaf nitrogen per unit area; N_E – Net ecosystem-atmosphere CO_2 exchange; NIR – Near-infrared radiation; p – Atmospheric pressure; P_b – Probability of no contact within a canopy layer for beam irradiance; P_d – Probability of no contact within a canopy layer for diffuse irradiance; PAR – Photosynthetic active radiation; q – Specific humidity; R_d – Respiration rate during the day but in the absence of photorespiration; $R_{d\_25} - R_d$ at 25 °C; R_{Lab} – Absorbed longwave radiation within a canopy layer; $R_{Labsl} - R_{Lab}$ of the sunlit leaves; $R_{Labsh} - R_{Lab}$ of the shaded leaves; R_s – Global solar radiation; R_{sabsl} – Total R_s absorbed by sunlit leaves; R_{sabsh} – Total R_s absorbed by shaded leaves; R_{sab_soil} – Total R_s absorbed by the soil surface; RSL – Roughness sub-layer; S_b – PAR or NIR at the given height for beam irradiance; S_c – Source strength for CO_2; S_d – PAR or NIR at the given height for diffuse irradiance; S_q – Source strength for water vapor; S_T – Source strength for heat; S_u – Momentum source; SVAT – Soil-vegetation-atmosphere transfer; t – Time; T – Air temperature at a given height; T_l – Leaf temperature; T_{soil} – Soil temperature; u – Wind speed; V_{cmax} – Maximum carboxylation rate when RuBP is saturated; $V_{cmax\_25} - V_{cmax}$ at 25 °C; w – Vertical wind speed; z – Height above the ground; z_r – Reference height; ε_l – Leaf emissivity; ε_s – Soil emissivity; η – Leaf transmissivity; λ – Latent heat of vaporization of water; λ_1 – Characteristic length scale for turbulent transport; λ_4 – Characteristic length scale for t pressure-scalar gradient correlation; λE_{soil} – Latent heat flux at the soil surface; ξ – Leaf reflectivity; ρ_a – Air density; σ – Stefan-Boltzmann constant; Ω – Clumping factor

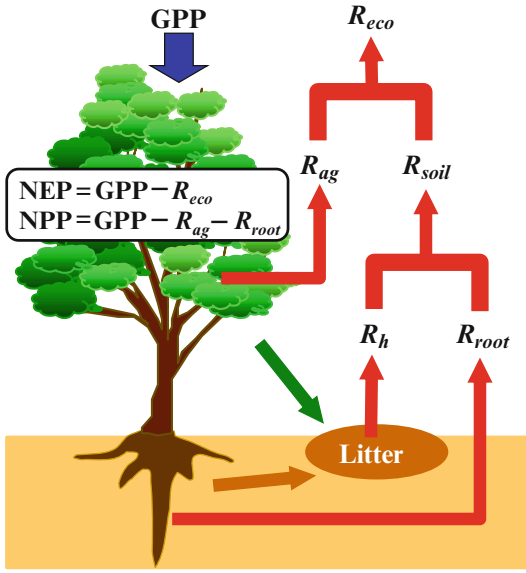

Fig. 10.1. Schematic representation of carbon flow in a forest. R_h, R_{root}, R_{ag}, R_{soil} and R_{eco} are respiratory fluxes from soil carbon, root, aboveground biomass, soil as a whole and ecosystem as a whole. Gross primary productivity (GPP) denotes carbon absorbed by the ecosystem as a whole. Thus, net ecosystem productivity (NEP; shown as GPP − R_{eco}) is ecosystem carbon sequestration, which can be directly measured by micrometeorological methods. Net primary productivity (NPP; shown as GPP − R_{ag} − R_{root}) means production (including litter) in the ecosystem

estimates can be compared with the ecosystem carbon budget estimated by summation of carbon flux components, which represents a valuable tool to clarify carbon flow processes in the ecosystem. Further, an appropriate period of flux observation reveals characteristics of diurnal, seasonal, interannual and interannual variations of CO_2 flux (i.e. vegetation productivity).

A combination of detailed observation of atmospheric and ecophysiological variables and the flux enables investigation of which factors control ecosystem CO_2 exchange. Furthermore, outputs from global and local models are independently validated using eddy covariance flux measured at the top of the canopy. We emphasize that such models were parameterized by independently collected ecophysiological measurements and were driven by observed or generated meteorological variables, and were not calibrated or parameterized by canopy-level flux measurements. After validation, such models can be used to examine how vegetation responds to climate change and, in turn, how functional vegetation changes induced by that change alter global and local climates.

In this review, I briefly describe eddy covariance measurement as the representative micrometeorological flux measurement method and its theory supporting measurements, with an explanation of their practice and limitations. In addition, I introduce the application of the Soil-Vegetation-Atmosphere Transfer (SVAT) model, which considers canopy microclimate processes such as radiation transfer, leaf-scale physiology, and turbulence within the canopy.

II. Theory of Measurement

A. Atmospheric Boundary Layer

Vertical profiles of wind speed, air temperature, and material concentrations vary drastically near the earth surface relative to their horizontal gradients, because of transport processes at the boundary of the domain of the atmosphere (Stull 1988). The atmospheric boundary layer (ABL) can be defined as the lowest part of the troposphere that is directly influenced by the earth surface characteristics (Fig. 10.2). ABL thickness is variable in time and space, ranging from a few tens of meters to several kilometers. All micrometeorological methods should be applied to the ABL, which can be divided into layers according to controlling factors of turbulent transport in each layer. Thus, examination of each ABL layer characteristics is useful for considering exchange processes between the surface and atmosphere.

Under neutral conditions, the convective boundary layer (CBL) is influenced by synoptic and mesoscale processes, whereas under unstable conditions, turbulence in the CBL is convectively driven. The intense

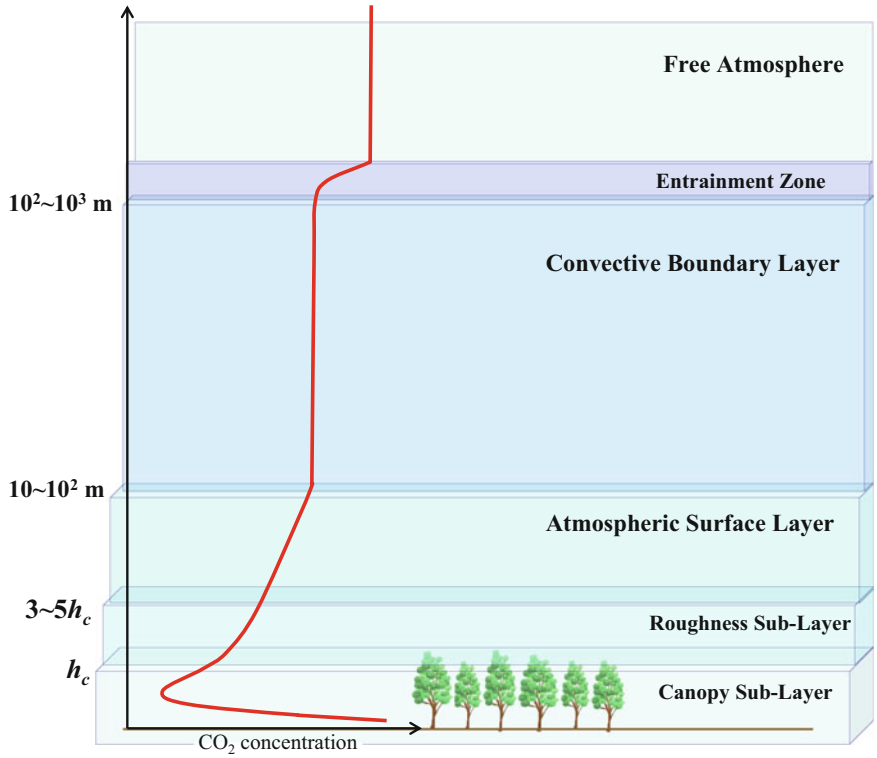

Fig. 10.2. The atmospheric boundary layer (*ABL*), consisting of two major layers, the convective boundary layer (*CBL*) and atmospheric surface layer (*ASL*). The remainder of the air in the troposphere is the free atmosphere. The ASL is subdivided into several sublayers, such as the roughness sublayer (*RSL*), canopy sublayer (*CSL*, where h_c is canopy height), and the remainder (referred to as the inertial sublayer). Typical daytime profile of mean CO_2 concentration is also shown

turbulence in the CBL tends to mix materials promptly and uniformly in the vertical (CO_2 concentration profile in Fig. 10.2). Such mixing causes weak vertical gradients of wind speed and direction and potential temperature. A stable layer at the CBL top is called the inversion layer or entrainment zone, which acts as a lid on convection in the CBL and is where entrainment from the free atmosphere into the CBL occurs.

There are vertical gradients of variables such as wind speed and materials concentration within the bottom 10 % of the ABL, which is called the atmospheric surface layer (ASL). The ASL is often referred to as the "constant flux layer," because vertical turbulent fluxes vary by less than 10 % of their magnitude in this layer. The height of the ASL bottom is about 3–5 times the representative height of the roughness element (h_c in Fig. 10.2; the forest canopy height here). The layer between heights h_c and 3–5 times h_c is called the roughness sublayer (RSL). In the layer beneath the RSL, the so-called canopy sublayer (CSL), turbulence is strongly influenced by the roughness element (i.e. trees) and reduced by viscosity. The CO_2 concentration profile in the CSL (Fig. 10.2) reveals the strongest sink of CO_2 at the mid-canopy position; a strong source, caused by soil respiration, is at the soil surface.

B. Eddy Flux

Fluid motion such as turbulence can transport materials in the atmosphere, resulting in fluxes. The turbulence is generated by eddies on various scales in the ABL. At a point where one observes an eddy flowing in a

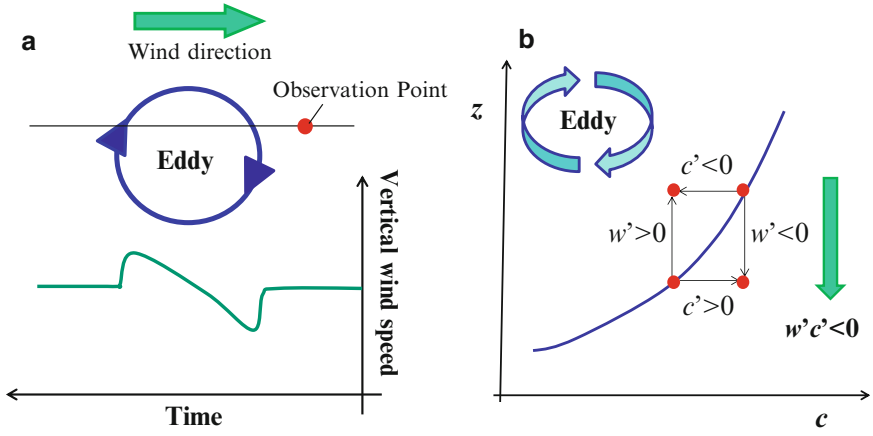

Fig. 10.3. (**a**) An eddy flowing to a given wind direction causes perturbations of vertical wind speed observed at a given position. (**b**) Schematic representation of the small eddy mixing process, showing net downward turbulent CO_2 flux. z, c, w, and prime denote height, CO_2 concentration, vertical wind speed, and perturbation part, respectively

direction, vertical wind speed fluctuates (Fig. 10.3a). This is the turbulence, which drives the vertical transport of materials. As seen in the figure, even though the materials are transported vertically, the dominant air parcel flow containing the materials is horizontal. Thus, the vertical flux at a given measurement height results from integration of the source/sink distribution of the flux on vegetation surfaces (Schuepp et al. 1990). Measurement over an extensive flat area upwind at a height sufficiently close to the vegetated surface would minimize the problem induced by a heterogeneous source/sink distribution on the surface, which is called the fetch problem.

Micrometeorological flux measurement methods were established based on eddy diffusivities. Thus, for appropriate measurements, one needs to take them above the RSL (where diffusivities are enhanced), so that the effect of heterogeneous terrain may not violate the assumption of a flat extensive area upwind (described later). However, by doing so, the fetch problem arises and small gradients of material concentration complicate flux measurement using eddy diffusivity theory. I emphasize that one cannot help in practice conducting tower-based flux measurement over tall vegetation (i.e. a forest canopy) within the RSL. Nonetheless, before commencing full-scale flux observation, one should consider a balance between measurement height and the fetch problem (Lloyd 1995).

Intrinsically, the vertical CO_2 flux (F_c: μmol m^{-2} s^{-1}) can be expressed as

$$F_c = \rho_a c \times w \tag{10.1}$$

where ρ_a, c, and w are air density (mol m^{-3}), CO_2 concentration (μmol mol^{-1} = ppmv) in the air, and vertical wind speed (m s^{-1}), respectively. Both c and w have fine fluctuations in their nature, and thus it is expedient to estimate net turbulent material flux by averaging the flux over a given period:

$$F_c = \overline{\rho_a wc} = \rho_a \overline{wc} \tag{10.2}$$

where the overbar denotes time averaging over a given period. c and w during the period are expressed by

$$\begin{aligned} c &= \overline{c} + c' \\ w &= \overline{w} + w' \end{aligned} \tag{10.3}$$

where the prime denotes a departure from the temporal averaging operator. The overbar

and prime components are called the mean and turbulent part, respectively. Substituting Eq. 10.3 for Eq. 10.2 gives

$$F_c = \rho_a \overline{(\overline{w} + w')(\overline{c} + c')} = \rho_a \left(\overline{wc} + \overline{w'}\,\overline{c} + \overline{w}\,\overline{c'} + \overline{w'c'} \right) \quad (10.4)$$

Assuming a flat extensive and heterogeneous terrain upwind and/or measurements above the RSL, one can make $\overline{w} = 0$ and $\overline{w'} = 0$ to obtain

$$F_c = \rho_a \overline{w'c'} \quad (10.5)$$

Application of Eq. 10.5 to the flux estimate is called the eddy covariance method, and requires fast response and high-frequency sampling sensors such as a sonic anemometer and closed-path or open-path analyzers. To understand the meaning of instantaneous product $w'c'$ and net flux $\overline{w'c'}$, it is instructive to examine a small idealized eddy near the vegetation surface during daylight hours (Fig. 10.3b). Average CO_2 concentration usually decreases toward the surface because of active absorption of CO_2 from the vegetation, i.e., photosynthesis. Assuming that the eddy is a swirling motion, some air parcels are mixed upward (positive w') and some mixed downward (negative w'). The upward ($w' > 0$) and downward ($w' < 0$) moving air parcels make the CO_2 concentration lower ($c' < 0$) or higher ($c' > 0$) than their surroundings, respectively. In both cases, the instantaneous product $w'c'$ is negative, indicating that both the upward and downward moving air parcels contribute negatively to the flux $w'c'$. Thus, the average eddy CO_2 flux $\overline{w'c'}$ is negative for this small eddy mixing process.

In practice, F_c cannot be obtained from simple calculation such as $\overline{w'c'}$, because there are some cases in which we cannot assume $\overline{w} = 0$. For example, complex terrain and vegetation structure (Kaimal and Finnigan 1994; Lee 1998; Lee et al. 2004) and changes of dry air density (Webb et al. 1980; Leuning 2007) cause nonzero $\overline{w}$ effects, and draw attention to the need to consider corrections of the measured flux. Hereafter in this chapter for simplicity, the notation $\overline{w'c'}$ will be used for F_c.

C. Above-Canopy Flux, Storage Flux, and Net Ecosystem Exchange

Since micrometeorological methods are based on fluid mechanics, one should begin with its fundamentals, i.e. an equation for scalar conservation (Baldocchi et al. 2000):

$$\frac{\partial \overline{\rho_a c}}{\partial t} = -\frac{\partial \left(\rho_a \overline{w'c'} \right)}{\partial z} + S_c(t,z) \quad (10.6)$$

where t is time (s), z is height (m) above the ground, and S_c is the source term (μmol m^{-3} s^{-1}) from mass absorption/release (i.e. net photosynthesis). Here, no lateral advection of CO_2 out of the sampling area is assumed. As delimited by the canopy height h_c, integrating Eq. 10.6 from the ground to reference height z_r gives

$$\int_0^{z_r} \rho_a \frac{\partial \overline{c}}{\partial t} dz = -\rho_a \left(\overline{w'c'}(z_r) - \overline{w'c'}(0) \right) + \int_0^{h_c} S_c(t,z) dz \quad (10.7)$$

where $\overline{w'c'}(z_r)$ and $\overline{w'c'}(0)$ are observed CO_2 fluxes at height z_r, called the above-canopy flux, and ground surface (i.e. soil respiration), respectively. The balance between the vertical integration of net photosynthesis and soil respiration is called net ecosystem CO_2 exchange N_E, and is given by

$$\rho_a \overline{w'c'}(0) + \int_0^{h_c} S_c(t,z) dz = N_E = \rho_a \overline{w'c'}(z_r) + \int_0^{z_r} \rho_a \frac{\partial \overline{c}}{\partial t} dz \quad (10.8)$$

Equation 10.8 suggests that N_E can be estimated from observation of the above-canopy flux (first term on right side of

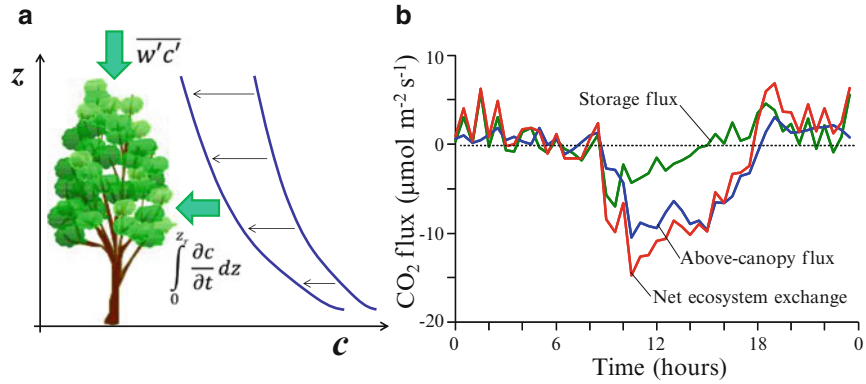

Fig. 10.4. (**a**) Representation of above-canopy flux and storage flux induced by change in vertical CO_2 concentration (c) profile. (**b**) Diurnal variations in above-canopy flux, storage flux, and net ecosystem exchange, observed in a Bornean tropical rainforest

Eq. 10.8) using the eddy covariance system on the canopy top and within-canopy storage flux (second term on right side of Eq. 10.8). The latter term is determined by quantifying the rate of change of CO_2 concentration in the air column within the canopy (Fig. 10.4a).

Observation in a Bornean tropical rainforest showed diurnal variations in the above-canopy flux, storage flux, and their sum, i.e. N_E (Fig. 10.4b). Most of the nocturnal-respired CO_2 at the rainforest site was stored within the canopy until morning, and was reabsorbed into the canopy through photosynthesis around 0800–1000 local time (LT). N_E represents a diurnal cycle of vegetation activity, and thus I address the physiological interpretation of N_E in relation to environmental factors, using the SVAT model.

III. Modeling

A. Soil-Vegetation-Atmosphere Transfer (SVAT) Model

Vegetation affects the within-canopy microclimate by intercepting radiation, attenuating wind, and distributing sources/sinks of materials and energy at each position within the canopy. These source/sink distributions and canopy turbulence form scalar distributions (air temperature, humidity, and CO_2 concentration) and above-canopy fluxes such as heat, H_2O, and CO_2. These scalar distributions in turn influence the within-canopy microclimate and scalar source/sink strength.

In reality, vegetation canopy fluxes form as a result of the aforementioned within-canopy processes (cf. Chap. 9, Hikosaka et al. 2016b). Therefore, I focus on a one-dimensional (vertical-only) multilayer SVAT model (Kumagai et al. 2006) that attempts to faithfully reproduce the formation process of eddy flux described in the previous part of this chapter. The model explicitly considers three major within-canopy processes: (1) radiative transfer and leaf-scale energy conservation; (2) leaf-scale ecophysiological status for stomatal opening and carbon assimilation; and (3) turbulent diffusion of materials (Baldocchi 1992). Detailed description of the turbulent transport process enables the SVAT model to reproduce the eddy flux measurements. For model computation, the canopy is divided into layers and all equations describing the within-canopy processes (1–3) are solved for each layer. The model used here was parameterized with independently collected ecophysiological measurements and was not calibrated or parameterized with canopy-level flux measurements.

1. Radiative Transfer and Energy Balance at Both Leaf and Soil-Surface Levels

When considering leaf-scale energy balance (cf. Chap. 2, Gutschick 2016) together with photosynthesis in a forest canopy, radiative transfer through the canopy (cf. Chap. 1, Goudriaan 2016) must be determined. Then, direct beam and diffuse irradiance must be considered separately, owing to their different attenuation in the canopy. The probability of no contact within a canopy layer for beam irradiance (P_b) must be formulated for describing direct irradiance transfer within the canopy. This formulation includes leaf area density (a_{leaf} in $m^2\ m^{-3}$), the beam extinction function of solar elevation, and leaf angle distribution within a given layer. When considering the effect of clumped foliage and crowns, we should incorporate a clumping factor (Ω) in the P_b equation by replacing a_{leaf} with Ωa_{leaf} (see Kumagai et al. 2013). The probability of no contact within a canopy layer for diffuse irradiance (P_d) is calculated by integrating P_b over the solid angles of the sky hemisphere.

Both direct and diffuse solar radiation can be further separated into photosynthetic active radiation (PAR) and near-infrared radiation (NIR), according to their different absorptions by leaves. Fortunately, approximately half the global solar radiation (R_s: W m^{-2}) over the canopy is in the form of PAR, while the other half is in the form of NIR. This enables estimates of R_s penetration inside the canopy. The absorbed PAR or NIR within a canopy layer between z (height above ground) and $z + \Delta z$, ΔS (W m^{-2}), is defined as

$$\Delta S_b = (1 - \eta - \xi)(1 - P_b)S_b(z + \Delta z) \quad (10.9)$$

$$\Delta S_d^{\downarrow} = (1 - \eta - \xi)(1 - P_d)S_d^{\downarrow}(z + \Delta z) \quad (10.10)$$

$$\Delta S_d^{\uparrow} = (1 - \eta - \xi)(1 - P_d)S_d^{\uparrow}(z) \quad (10.11)$$

where η and ξ are leaf transmissivity and reflectivity, respectively, for PAR or NIR. S is PAR or NIR at the given height (W m^{-2}). Subscripts b and d denote direct beam and diffuse irradiation, respectively, and superscript arrows indicate the direction of the irradiation. Although it appears that Eqs. 10.9, 10.10, and 10.11 are simple formulations of the two-stream model, P_b and P_d are complex functions of a_{leaf}, leaf angle distribution and Ω within a given canopy layer and solar geometric direction. Therefore, this shortwave radiative transfer model can be considered a semi-3D model (see Kumagai et al. 2006). Total absorbed solar radiation within the canopy layer is then calculated as the sum of absorbed PAR and NIR, both of which are calculated by Eqs. 10.9, 10.10 and 10.11. Sunlit leaves receive the beam and upward and downward diffuse radiation, while shaded leaves receive only upward and downward diffuse radiation. Therefore, irradiance absorption and energy balance must be computed separately for sunlit and shaded leaves.

The absorbed long-wave radiation within a canopy layer between z and $z + \Delta z$, R_{Lab} (W m^{-2}), is defined as

$$R_{Lab} = (1 - P_d)L^{\uparrow}(z) + (1 - P_d)L^{\downarrow}(z + \Delta z) \quad (10.12)$$

Here, L is long-wave radiation at the given height (W m^{-2}), calculated using leaf temperature (T_l in K) and the theory for diffuse irradiance transfer within the canopy layer between z and $z + \Delta z$ (Kumagai et al. 2006).

Energy balance at the soil surface for computing soil temperature (T_{soil} in K) is expressed by

$$R_{sab\_soil} + L^{\downarrow}(0) - \varepsilon_s \sigma {T_{soil}}^4 = \lambda E_{soil} + H_{soil} \quad (10.13)$$

where R_{sab_soil} is the total R_s absorbed by the soil surface (W m^{-2}), ε_s is soil emissivity, σ is the Stefan-Boltzmann constant (5.67×10^{-8} W m^{-2} K^{-4}), and λE_{soil} and H_{soil} are latent (W m^{-2}) and sensible (W m^{-2}) heat fluxes at the soil surface, respectively. λE_{soil} and H_{soil} are functions of T_{soil}, as described by the products of

transport conductance and concentration difference. In addition, soil-surface moisture availability was used for λE_{soil} conductance. For full computations describing λE_{soil} and H_{soil}, a more complicated soil physics describing soil heat and water motion is needed (Campbell and Norman 1998).

The energy balance on sunlit and shaded leaf surfaces within a canopy layer between z and $z + \Delta z$ is expressed by

$$R_{sabsl} + R_{Labsl} - 2(1 - P_d)\varepsilon_l \sigma {T_{lsl}}^4 a_{sl}/a_{leaf} = \lambda E_{lsl} a_{sl} \Delta z + H_{lsl} a_{sl} \Delta z \quad (10.14)$$

$$R_{sabsh} + R_{Labsh} - 2(1 - P_d)\varepsilon_l \sigma {T_{lsh}}^4 a_{sh}/a_{leaf} = \lambda E_{lsh} a_{sh} \Delta z + H_{lsh} a_{sh} \Delta z \quad (10.15)$$

Here, R_{sabsl} and R_{sabsh} are total R_s absorbed by sunlit and shaded leaves, respectively (W m^{-2}), expressed per unit of ground area. R_{Labsl} and R_{Labsh} are R_{Lab} of the sunlit and shaded leaves (W m^{-2}) within a canopy layer between z and $z + \Delta z$, respectively, expressed per unit of ground area. ε_l is leaf emissivity, and subscripts *sl* and *sh* denote sunlit and shaded leaves, respectively. a_{sl} and a_{sh} are sunlit and shaded leaf area densities (m^2 m^{-3}) within a given layer, respectively. λ is the latent heat of vaporization of water (J kg^{-1}), and E_l and H_l respectively represent water vapor (kg m^{-2} s^{-1}) and sensible heat (W m^{-2}) fluxes expressed per unit of leaf area. These are described in the next section. The energy balance Eqs. 10.14 and 10.15 are critical for computation of T_l, which is required for assessing leaf physiological activity as follows.

2. Leaf-Level Physiological Functions

Leaf-level scalar source strengths, i.e., leaf sensible heat (H_l in W m^{-2}), transpiration (E_l in kg m^{-2} s^{-1}) and photosynthesis rate (A_l in μmol m^{-2} s^{-1}), are derived from physiological controls using

$$H_l = 2 m_a c_p g_{ah} (T_l - T) \quad (10.16)$$

$$E_l = m_e g_w \frac{[e_{sat}(T_l) - e]}{p} \quad (10.17)$$

$$A_l = g_{ac}(c - C_s) \quad (10.18)$$

$$= g_{sc}(C_s - C_i) \quad (10.19)$$

where m_a and m_e are the molecular weights of air and water (kg mol^{-1}), respectively, c_p is the specific heat of air at constant pressure (J kg^{-1} K^{-1}), and g_{ah}, g_{ac} and g_w are boundary conductances for heat and CO_2 and total conductance for water vapor (mol m^{-2} s^{-1}), respectively. T is air temperature (K) at a given height, and $e_{sat}(T_l)$ and e are saturation vapor pressure at leaf temperature (T_l) and atmospheric water vapor pressure (Pa), respectively. p is atmospheric pressure (Pa), and C_s, c and C_i are CO_2 concentrations (μmol mol^{-1}) of air inside and outside the laminar boundary layer of leaves and within the stomatal cavity, respectively. g_w is the sum of the reciprocals of the stomatal (g_{sw}, mol m^{-2} s^{-1}) and boundary layer (g_{aw}, mol m^{-2} s^{-1}) conductances for water vapor. Campbell and Norman (1998) gave typical formulations of boundary conductances.

As described by Ball et al. (1987) and Collatz et al. (1991), g_{sc} is stomatal conductance for CO_2 (mol m^{-2} s^{-1}) and is linked to A_l, the relative humidity of air inside the boundary layer of a leaf (h_s), and C_s:

$$g_{sc} = m_L \frac{A_l h_s}{C_s} + b_L \quad (10.20)$$

where m_L and b_L are the slope and intercept, respectively. These were obtained by linear regression of data from leaf-level gas exchange measurements. g_{sw} was obtained from $g_{sw} = 1.6\, g_{sc}$, where 1.6 is the ratio of diffusivities of water and CO_2 in air (von Caemmerer and Farquhar 1981).

A_l was computed using the biochemical model of Farquhar et al. (1980) and Collatz

et al. (1991) as a minimum value of the gross rate of photosynthesis, limited by the rate of ribulose bisphosphate (RuBP) regeneration through electron transport (J_E in μmol m^{-2} s^{-1}), RuBP carboxylase/oxygenase (Rubisco) activity (J_C in μmol m^{-2} s^{-1}), and the export rate of synthesized sucrose (J_S in μmol m^{-2} s^{-1}), as

$$A_l = \min\{J_E, J_C, J_S\} - R_d \tag{10.21}$$

Here, R_d is the respiration rate (μmol m^{-2} s^{-1}) during the day but in the absence of photorespiration. The formulations and parameterizations of J_E, J_C, J_S and R_d as a function of PAR absorbed by the leaf, CO_2 concentration within the stomatal cavity, and leaf temperature (T_l) are given in Chap. 3 (Hikosaka et al. 2016a) of this volume. In those formulations, the maximum carboxylation rate when RuBP is saturated (V_{cmax} in μmol m^{-2} s^{-1}), the potential rate of whole-chain electron transport (J_{max} in μmol m^{-2} s^{-1}), and R_d are critical sub-functions, which are expressed as nonlinear functions of T_l and values at 25 °C (V_{cmax_25}, J_{max_25}, and R_{d_25}, respectively). Practically, both J_{max_25} and R_{d_25} are related to V_{cmax_25}. Hence, V_{cmax_25} is the key parameter in the leaf photosynthesis model.

The aforementioned model calculates A_l for both sunlit and shaded leaves. The A_l calculated in Eq. 10.21 is coupled with g_{sc} using Eq. 10.20. Hence, determination of A_l requires C_s, C_i, h_s and T_l, which result from e, c and T using Eqs. 10.16, 10.17, 10.18, and 10.19. Thus, all three scalar (e, c and T) transport equations and Eqs. 10.16, 10.17, 10.18, and 10.19 must be simultaneously considered, as described in the following.

3. Scalar Transport

Scalar continuity is obtained assuming steady-state planar homogeneity (cf. Eq. 10.6):

$$\frac{d\varphi}{dt} = 0 = -\frac{d\overline{w'\varphi'}}{dz} + S_\varphi(t,z) \tag{10.22}$$

where φ is a variable such as T, specific humidity (q in kg kg^{-1}) or c, and $\overline{w'\varphi'}$ is the vertical turbulent flux. S_φ is a source (or sink) term for φ, attributable to mass release (or uptake) by the ensemble of leaves within the averaging plane, given by

$$S_T = \frac{1}{m_a \rho_a c_p}\left(H_{lsl}a_{sl} + H_{lsh}a_{sh}\right) \tag{10.23}$$

$$S_q = \frac{1}{m_a \rho_a}\left(E_{lsl}a_{sl} + E_{lsh}a_{sh}\right) \tag{10.24}$$

$$S_c = -\frac{1}{\rho_a}\left(A_{lsl}a_{sl} + A_{lsh}a_{sh}\right) \tag{10.25}$$

where S_T, S_q, and S_c are source strengths for heat (K s^{-1}), water vapor (kg kg^{-1} s^{-1}), and CO_2 concentration (μmol mol^{-1} s^{-1}), respectively.

To compute φ, S_φ and $\overline{w'\varphi'}$, use of a turbulent diffusion model is required and two main approaches have been adopted, Lagrangian and Eulerian models (see Katul and Albertson 1999). In the Lagrangian dispersion model, scalar concentration differences between arbitrary and reference heights were computed by summing the contributions of scalar diffusion to or from various canopy heights, expressed by a dispersion matrix calculated using the random walk algorithm (see Baldocchi 1992; Baldocchi and Meyers 1998). The Lagrangian approach has been successfully used to compute the interdependence between scalar sources and concentrations and resultant fluxes (e.g. Raupach 1988; Baldocchi 1992; Lai et al. 2000).

With regard to the Eulerian approach, the closure approximation is required to prevent an increase in the order of the turbulent flux term. Assuming that the turbulent Schmidt number for scalar is unity, one can apply a first-order turbulent closure scheme (see Kumagai et al. 2013):

$$\overline{w'\varphi'} = -K_t \frac{d\varphi}{dz} \tag{10.26}$$

where K_t is eddy turbulent diffusivity ($m^2\ s^{-1}$). In general, the first-order closure principles fail in countergradient flows but are applicable when the production term is balanced by the dissipation term in the scalar flux budget, with minimal contributions from gradients in the turbulent flux transport terms (see Manzoni et al. 2011).

Both Lagrangian and higher-order Eulerian approaches can be formulated to account for the existence of countergradient flow (see Katul and Albertson 1999). Here, assuming steady-state planar homogeneity and high Reynolds number and Peclet number flow, and applying temporal and horizontal averaging, the turbulent vertical flux equation for φ with a second-order closure scheme is (see Katul and Albertson 1999):

$$0 = -\overline{w'^2}\frac{d\varphi}{dz} + 2\frac{d}{dz}\left(e_{tk}\lambda_1\frac{d\overline{w'\varphi'}}{dz}\right) - \frac{e}{3\lambda_4}\overline{w'\varphi'} \tag{10.27}$$

where e_{tk} is a turbulent kinetic energy, and λ_1 and λ_4 are characteristic length scales for turbulent transport and pressure-scalar gradient correlation, respectively (see Watanabe 1993).

To solve Eqs. 10.22, 10.23, 10.24, 10.25, 10.26 or 10.22, 10.23, 10.24, 10.25, and 10.27, velocity statistics within the canopy must be computed. For the first-closure model, we have only to substitute u (wind speed in m s^{-1}) for φ in Eqs. 10.22 and 10.26 and use a momentum source $S_u = C_d\ a_{leaf}\ u^2$, where C_d is the drag coefficient (see Kumagai et al. 2013). For the second-order closure model for turbulent vertical fluxes, the second-order closure model for canopy turbulence formulated by Wilson and Shaw (1977) is generally applied. Then, boundary conditions can be specified in accord with Katul and Albertson (1999), and the closure constants in Wilson and Shaw (1977), Watanabe (1993) and Katul and Albertson (1999) can be used. To solve the second-order closure model, the numerical scheme described in Katul and Albertson (1998, 1999) is applicable.

B. Model Applications

Again, the SVAT model introduced here is parameterized by independently collected data of ecophysiological traits such as V_{cmax_25} and m_L and of canopy structure such as a_{leaf} spatial variation, and is not calibrated or parameterized by canopy-level flux measurements. Model outputs are independently validated using the N_E measurements. After validation, the model can be used to examine how the energy and material fluxes over the forest ecosystems are generated, e.g. how the canopy structure and physiological traits impact CO_2 exchange between the canopy and atmosphere, shown by the following.

It is first necessary to validate the model by examining how sensitive the flux calculations are to micrometeorological factors. Examples of comparisons between modeled and measured N_E in a Bornean tropical rainforest (Kumagai and Kume 2012) are shown under four typical meteorological conditions. These are a rainfall event at noon (Fig. 10.5a, e), rainfall event from midnight to early morning and cloud during daylight hours (Fig. 10.5b, f), cloudy with little rainfall (Fig. 10.5c, g), and midnight rainfall and clear sky during daylight hours (Fig. 10.5d, h). There were two types of abrupt declines of N_E and solar radiation (R_s) at noon on 6 September with rainfall (Fig. 10.5a, e) and 11 September without rainfall (Fig. 10.5c and g). The model accurately reproduced measured N_E for the entire available data period, including periods of the four aforementioned meteorological conditions. Regression statistics for comparisons between measured and modeled values during daylight hours had a slope of 0.79, intercept of –0.80 μmol $m^{-2}\ s^{-1}$, R^2 of 0.62, and a root mean square error of 6.95 μmol $m^{-2}\ s^{-1}$ (Kumagai et al. 2006).

Measurements of horizontal variation of leaf area index (LAI) at the tropical rainforest site revealed values from 4.8 to 6.8 $m^2\ m^{-2}$, with a mean of 6.2 $m^2\ m^{-2}$. Cumulative LAI data measured downwards from the canopy top at 57 observation points

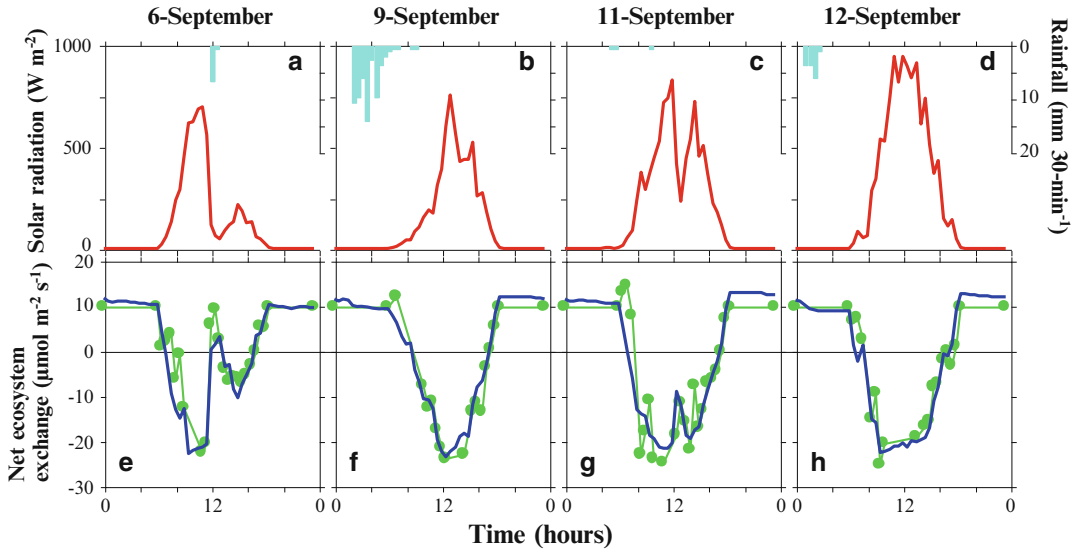

Fig. 10.5. Diurnal patterns of rainfall (*bars*) and solar radiation (*lines*) (**a–d**), and measured (*closed circles*) and modeled (*lines*) net ecosystem CO_2 exchange (**e–h**) in Bornean tropical rainforest from 6 to 12 September 2002 (From Kumagai and Kume 2012)

along four vertical lines showed a strong linear relationship between z and cumulative LAI ($R^2 = 0.82$). A straight line representing this linear relationship, connecting two points (z, cumulative LAI) = (0, LAI) and (h, 0), can be generated by integrating constant vertical distributions of leaf area density. Hence, Kumagai et al. (2006) assumed that LAI varied horizontally at the site between 4.8 and 6.8 $m^2\ m^{-2}$, and that at each horizontal position, leaf area density was vertically constant from the canopy top to forest floor. Because in describing variation of leaf-level physiological parameters we had only to present the one-dimensional vertical variation (Kumagai et al. 2006), how the flux calculations respond to changes in vertical distributions of leaf area density should also be examined. Thus, Kumagai et al. conducted four numerical experiments with consideration of the results of leaf area density. In Case 1, a mean observed LAI of 6.2 $m^2\ m^{-2}$, along with constant leaf area density of 0.123 $m^2\ m^{-3}$ from the canopy top to forest floor, was used in the SVAT model. Cases 2 and 3 assumed LAIs of 6.8 and 4.8 $m^2\ m^{-2}$ (the maximum and minimum observed LAIs), along with constant leaf area densities of 0.136 and 0.096 $m^2\ m^{-3}$, respectively. In most SVAT models, the leaf area density distribution is arbitrarily assumed as a single vertical profile, because a tower is generally used to obtain measurements (however, Kumagai et al. used a canopy crane, which enabled them to obtain a 3D canopy structure). To examine the effect of arbitrarily determined vertical distributions of leaf area density on flux calculations, we also constructed Case 4, assuming a vertical distribution of leaf area density as a single vertical observation line, the LAI of which was 4.8 $m^2\ m^{-2}$.

In the study of Kumagai et al. (2006), all cases recreated the canonical form of measured N_E throughout all photosynthesis periods, implying that efforts to measure the detailed leaf area density distribution within the canopy do not always improve the predictive accuracy of the model. Reproducing both spatial and temporal patterns of the mean concentration field, a state variable influenced by combined source variation and turbulent transport mechanics, is one of the strengths of a multilayer SVAT model (Lai et al. 2000). However, although the

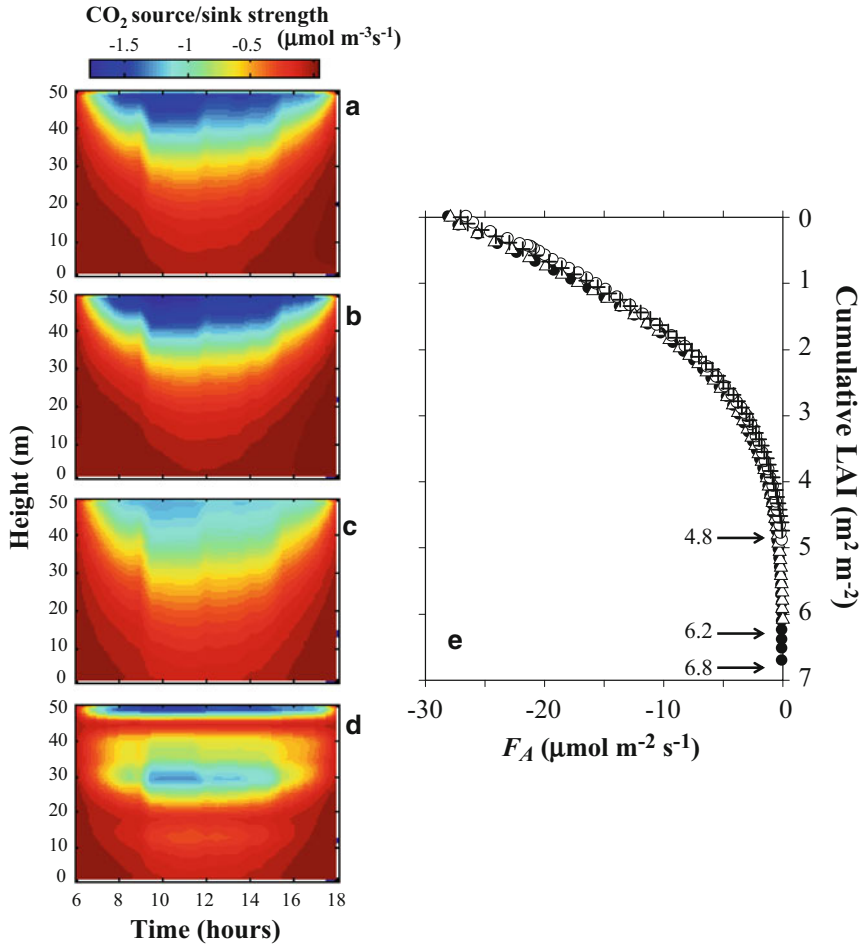

Fig. 10.6. Left panels: contour plots of average CO_2 source/sink distributions within the canopy as a function of height and time of day for Cases 1 (**a**), 2 (**b**), 3 (**c**), and 4 (**d**). *Right panel*: (**e**) vertical profiles of average CO_2 flux without soil respiration (F_A) around noon (1100–1300 LT) as a function of cumulative leaf area index (LAI) modeled from Cases 1 (*open triangles*), 2 (*closed circles*), 3 (*crosses*), and 4 (*open circles*). LAI values (6.8, 6.2 and 4.8) are also shown (From Kumagai et al. 2006)

model calculations of N_E clearly reproduced the measurements, those of the scalar profiles inside the canopy did not match the measured values. This implies that a simpler description of velocity statistics that modulate turbulent transport, like those proposed by Baldocchi and Meyers (1998), might be adequate.

At different levels in the canopy, absorbed radiation altered by changes in the vertical distribution of leaf area density mainly drives variations of physiological sources and sinks. Thus, Kumagai et al. (2006) compared CO_2 source strength distributions estimated with Cases 1–4. Figure 10.6a–d shows contour maps of these distributions as a function of time of day and height. In contrast to the calculated N_E, there were pronounced discrepancies between the estimated source strength distributions. Among Cases 1–3 (Fig. 10.6a–c, respectively), those with higher LAI had greater CO_2 uptake in the upper canopy layers, but less uptake in the lower canopy. In contrast, in Case 4 (Fig. 10.6d), CO_2 uptake was high at heights of about 50 and 30 m, where leaf area densities were also high.

Figure 10.6e compares profiles of average CO_2 flux without soil respiration (F_A) around

noon (1100–1300 LT) modeled from Cases 1–4, described as a function of cumulative LAIs measured downward from the canopy top. F_A denotes CO_2 flux in each canopy layer, expressed per unit area of ground. Therefore, F_A at cumulative LAI = 0 is equal to the above-canopy flux without soil respiration, and decreases with increasing cumulative LAI. The cumulative LAI is not necessarily related to canopy height. In contrast to the source strength distributions, there were no large differences between flux profiles of each case. This figure reveals that in Cases 1 and 2, which had high LAI, CO_2 uptake by leaves in the lower canopy layers contributed little to F_A because of the small contribution of J_E (see Eq. 10.21) in the lower canopy. Therefore, despite the varying distributions of leaf area density, a greater part of the above-canopy flux was generated by a constant cumulative LAI integrated from the canopy top, ~4.8 m^2 m^{-2}. Hence, the above-canopy flux appears robust to changes of leaf area density distributions, and in all cases the results were almost identical.

Given the strong vertical gradients of leaf photosynthetic capacity in tropical forest canopies, it is instructive to investigate the impacts of these vertical gradients on the CO_2 flux. This might be of use in framing a strategy for measuring leaf-level physiological parameters, because it is relatively difficult to access some positions within the canopy. Leaf nitrogen per unit area (N_a in g m^{-2}) is a key physiological parameter in the SVAT model (see Niinements and Tenhunen 1997; Wilson et al. 2001; Kumagai et al. 2006). At the study site, average N_a across species in height classes 0–5 m (30 individuals) and 40–55 m (10 individuals) were 0.68 (±0.25 standard deviation) and 1.41 (±0.14) g m^{-2}, respectively. Using the vertical distribution of leaf area density in Case 1, Kumagai et al. constructed two further numerical experiments, Cases 5A and B, which had constant vertical distributions of N_a (0.68 and 1.41 g m^{-2}, respectively). That is, Cases 5A and B assumed that N_a measured in the lower and upper canopies, respectively, was distributed evenly throughout, and evaluated CO_2 flux variation caused by these two "end-members" of vertical distribution with the assumption that the entire profile represents the N_a in either the lower or upper canopy. Figure 10.7a compares N_E modeled from Cases 1, 5A and 5B, bin-averaged by time of day. Although N_E in Case 5A was about half that in Case 1, that in Case 5B was nearly the same as in Case 1. This result also suggests that the N_a distributed through the canopy in Case 5B had no photosynthetic capacity in the lower canopy layers.

Distinct peaks of the diurnal precipitation cycle at specific times of the day at various locations in the Southeast Asian tropics have been found (Kumagai and Kume 2012). Because exchanges between forest canopy and atmosphere such as assimilation and evapotranspiration are driven mainly by solar radiation, their activities might be influenced by diurnal precipitation timing via the effects of weak incident solar radiation, low vapor-pressure deficit, and leaf wetness. Therefore, Kumagai and Kume investigated potential changes of N_E caused by alteration of diurnal rainfall regime. N_E was computed by the SVAT model with input of a 30-min interval rainfall time series. This series was constructed using rainfall statistics of observation site data (at Lambir) and published data of long-term diurnal precipitation cycles (at Bintulu and Kuching) in Borneo (Fig. 10.7b). For these computations, the authors replaced only rainfall temporal patterns (including rainfall amount) of Lambir with those of Bintulu and Kuching, and retained relationships between rainfall intensity and other environmental factors (such as R_s) as at Lambir. The highest rainfall peak in the diurnal rainfall cycle at Lambir resulted in the lowest N_E around 1300–1400 LT at the three sites, but the difference was very slight. There were also differences in N_E variability among those sites (e.g. at 1030 and 1500 LT), but these were very slight (Fig. 10.7b). As a result, there was little or no difference in the full-year N_E among the sites (Fig. 10.7b). This

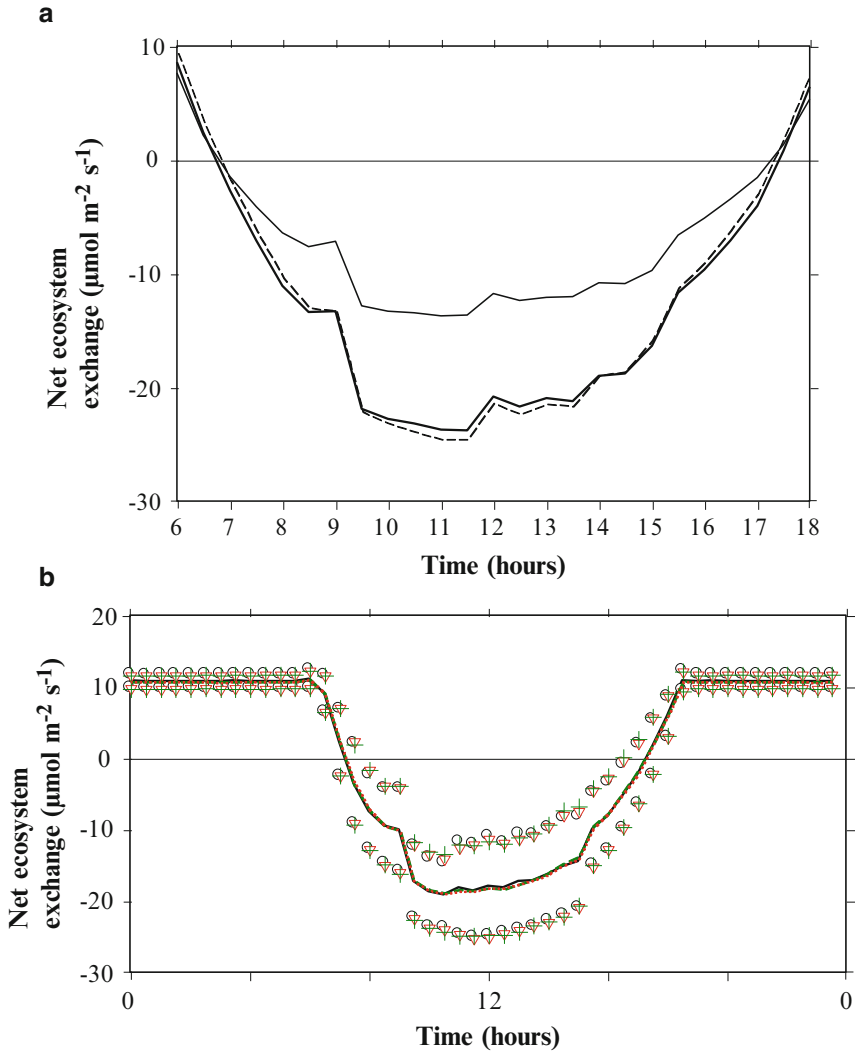

Fig. 10.7. (**a**) Average temporal variation of CO_2 fluxes (F_c) modeled from Cases 1 (*thick solid line*), 5A (*thin solid line*), and 5B (*broken line*). Cases 5A and B included constant vertical distributions of N_a (0.68 and 1.41 g m^{-2}, respectively) (From Kumagai et al. (2006)) (**b**) Average diurnal variations of modeled ecosystem CO_2 exchange for entire year with ± 1 standard deviation (SD) at Lambir (*solid line with circles*), Bintulu (*dotted line with triangles*), and Kuching (*broken line with crosses*) in Sarawak, Malaysia. Upper and lower symbols denote plus and minus one SD, respectively. All three lines almost perfectly overlap (From Kumagai and Kume 2012)

confirms that the diurnal rainfall cycle does not significantly affect the diurnal cycle of incident radiative energy in the studied tropical rainforest region. This is because the contribution of rainfall duration to the total duration is small, and productivity of the tropical rainforest ecosystem may be somewhat conservative in terms of its similarity across that region. This is because of the combined effects of N_E light response saturation at relatively low light intensity and constant cloud cover (Kumagai and Kume 2012).

Finally, to show the impact of canopy structure on atmosphere-canopy exchange, simulations of ecosystem CO_2 (N_E) and latent heat (LE) fluxes at a Cambodian rubber plantation site were conducted with

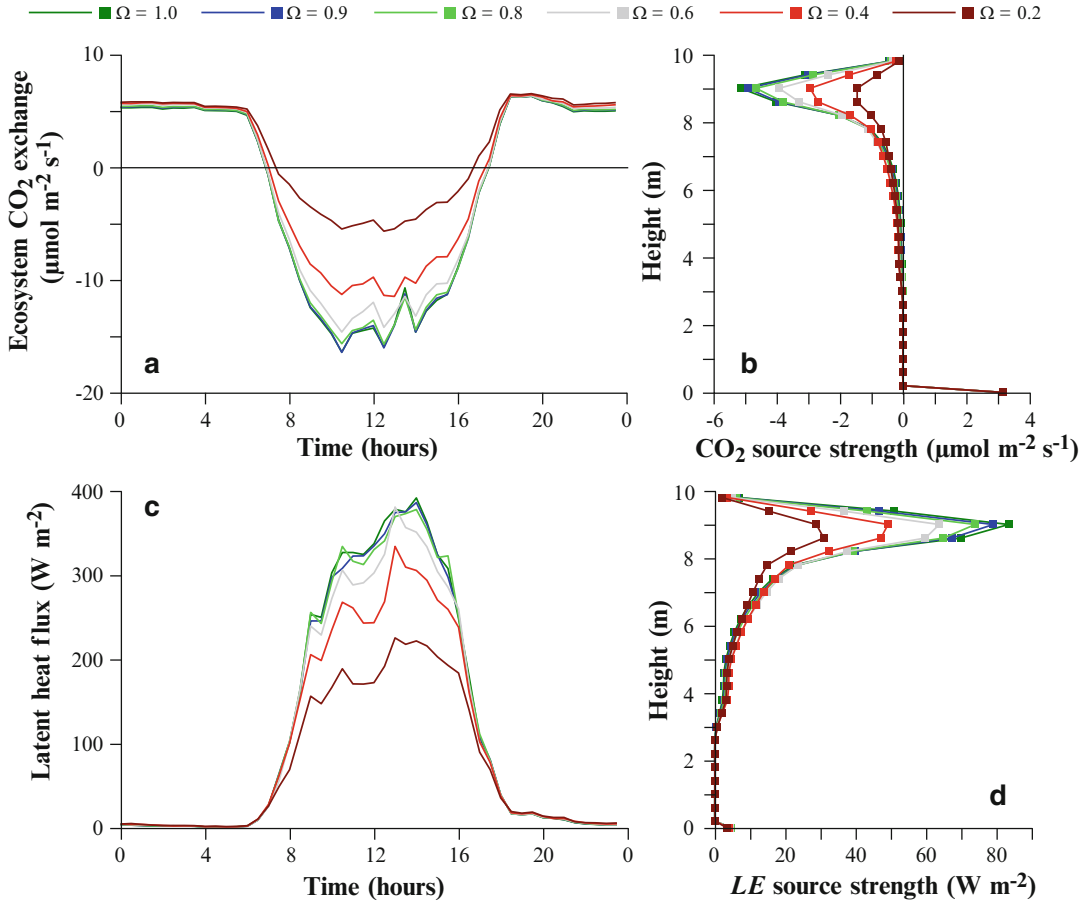

Fig. 10.8. Mean diurnal cycles of modeled ecosystem CO_2 exchange (**a**) and latent heat flux (*LE*) (**c**), along with vertical profiles of average modeled midday (1100–1300 LT) CO_2 (**b**) and *LE* (**d**) source strength as a function of canopy height, for canopy clumping factors (Ω) of 1.0, 0.9, 0.8, 0.6, 0.4 and 0.2. Total leaf area per ground area (LAI) was held constant at 3.89 (From Kumagai et al. 2013)

varying canopy clumping factors (Ω) and constant LAI (Kumagai et al. 2013). A decrease in Ω from 1.0 to 0.8 had little effect on either N_E and *LE* flux, but reducing Ω to less than 0.6 changed them appreciably (Fig. 10.8a, c). With decreasing Ω, fluctuations of N_E and *LE* fluxes at timescales shorter than the diurnal cycle became smaller and larger, respectively. In particular, *LE* flux tended to be depressed in the morning and rose in the afternoon (Fig. 10.8c). Figure 10.8b, d show that decreases in source strengths at their peaks in accord with decreases in Ω reduced N_E and *LE* fluxes. With decreasing Ω, source strengths in the upper canopy declined, while those in the lower canopy slightly increased. This implies that a Ω decrease enables light to penetrate deeper into the canopy. However, in the present study, strong source strengths in the upper canopy controlled the ecosystem fluxes because of dense foliage there (Fig. 10.8b, d).

IV. Future Research Directions

Prediction of carbon sequestration by vegetation under an increased atmospheric CO_2 environment and concomitant modifications to global climate are among the most important issues surrounding global climate

change, because global terrestrial ecosystem CO_2 absorption may impact local and global climate via direct atmospheric CO_2 concentration change. Also, vegetation covers a major part of the land surface and promotes latent heat exchange via transpiration. How the available energy is partitioned between sensible and latent heat fluxes at the air-land interface is critical for the evolution of local and global climate.

There are various relationships between global climatic factors and terrestrial ecosystem CO_2 dynamics. The climatic zone mainly determines vegetation type and thereby regional limitations on vegetation material exchange. The micrometeorological factors alter leaf-scale material exchange through environmental control of assimilation/respiration and stomatal aperture. Furthermore, extreme and drastic climatic shifts induce rapid and large-scale shifts in ecosystem structure and function, such as tree mortality and die-offs. This results in drastic changes in carbon, water and energy exchange between atmosphere and vegetation surfaces.

Again, our main concern is to gain the ability to predict global ecosystem carbon sequestration under climate change. Toward this objective, large-scale and long-term assessments of relationships between net ecosystem exchange (N_E) / net primary productivity and environmental factors are urgently needed. First of all, global investigations of N_E characteristics could be done using tower eddy covariance and meteorological data from the FLUXNET data archive (http://www.fluxnet.ornl.gov/). Also needed are an improved network of observations (e.g. a global network of vegetation inventories), which would be useful to clarify relationships between N_E and vegetation dynamics, and for validation of eddy flux data (see Chap. 12, Ohtsuka et al. 2016).

Combination of the SVAT model and the aforementioned network datasets would be a promising tool to generalize N_E characteristics of each vegetation type at global scale. Global and temporal patterns of environmental factors would permit straightforward construction of a global carbon balance map. Examples of such patterns could be basic climatic variables on a global 0.25° latitude-longitude resolution grid from the National Centers for Environmental Prediction – National Center for Atmospheric Research (NCEP-NCAR) reanalysis (cf. Kistler et al. 2001) and soil moisture outputs from the second Global Soil Wetness Project (GSWP-2) (cf. Dirmeyer et al. 2006).

Acknowledgments

I am grateful to the Forestry Department of Sarawak for their support during data acquisition. I also thank numerous colleagues who helped me with the eddy covariance works that I have ever done. The work was supported in part by a grant from the project "Program for Risk Information on Climate Change" of the Ministry of Education, Science and Culture, Japan.

References

Baldocchi D (1992) A Lagrangian random-walk model for simulating water vapor, CO_2 and sensible heat flux densities and scalar profiles over and within a soybean canopy. Bound Layer Meteorol 61:113–144

Baldocchi D, Meyers T (1998) On using eco-physiological, micrometeorological and biogeochemical theory to evaluate carbondioxide, water vapor and trace gas fluxes over vegetation: a perspective. Agric For Meteorol 90:1–25

Baldocchi D, Finnigan J, Wilson K, Paw UKT, Falge E (2000) On measuring net ecosystem carbon exchange over tall vegetation on complex terrain. Bound Layer Meteorol 96:257–291

Ball JT, Woodrow IE, Berry JA (1987) A model predicting stomatal conductance and its contribution to the control of photosynthesis under different environmental conditions. In: Biggens J (ed) Progress in Photosynthesis Research. Mirtinus Nijhoff Publishers, Dordrecht, pp 221–224

Campbell GS, Norman JM (1998) An Introduction to Environmental Biophysics. Springer, New York

Collatz GJ, Ball JT, Grivet C, Berry JA (1991) Regulation of stomatal conductance and transpiration: a physiological model of canopy processes. Agric For Meteorol 54:107–136

Dirmeyer PA, Gao X, Zhao M, Guo Z, Oki T, Hanasaki N (2006) The Second Global Soil Wetness Project (GSWP-2): multi-model analysis and implications for our perception of the land surface. Bull Am Meteorol Soc 87:1381–1397

Farquhar GD, von Caemmerer S, Berry JA (1980) A biochemical model of photosynthetic CO_2 assimilation in leaves of C3 species. Planta 149:78–90

Goudriaan J (2016) Light distribution. In: Hikosaka K, Niinemets Ü, Anten N (eds) Canopy Photosynthesis: From Basics to Applications. Springer, Berlin, pp 3–22

Gutschick VP (2016) Leaf energy balance: basics, and modeling from leaves to Canopies. In: Hikosaka K, Niinemets Ü, Anten N (eds) Canopy Photosynthesis: From Basics to Applications. Springer, Berlin, pp 23–58

Hikosaka K, Noguchi K, Terashima I (2016a) Modeling leaf gas exchange. In: Hikosaka K, Niinemets Ü, Anten N (eds) Canopy Photosynthesis: From Basics to Applications. Springer, Berlin, pp 61–100

Hikosaka K, Kumagai T, Ito A (2016b) Modeling canopy photosynthesis. In: Hikosaka K, Niinemets Ü, Anten N (eds) Canopy Photosynthesis: From Basics to Applications. Springer, Berlin, pp 239–268

Kaimal JC, Finnigan JJ (1994) Atmospheric Boundary Layers Flows. Their Structure and Measurement. Oxford University Press, New York

Katul GG, Albertson JD (1998) An investigation of higher-order closure models for a forested canopy. Bound Layer Meteorol 89:47–74

Katul GG, Albertson JD (1999) Modeling CO_2 sources, sinks, and fluxes within a forest canopy. J Geophys Res 104:6081–6091

Kistler R, Kalnay E, Collins W, Saha S, White G, Woollen J, Chelliah M, . . ., Fiorino M (2001) The NCEP-NCAR 50-year reanalysis: Monthly means CD-ROM and documentation. Bul Am Met Soc 82:247–267

Kumagai T, Kume T (2012) Influences of diurnal rainfall cycle on CO_2 exchange over Bornean tropical rainforests. Ecol Model 246:91–98

Kumagai T, Ichie T, Yoshimura M, Yamashita M, Kenzo T, Saitoh TM, Ohashi M, . . ., Komatsu H (2006) Modeling CO_2 exchange over a Bornean tropical rain forest using measured vertical and horizontal variations in leaf-level physiological parameters and leaf area densities. J Geophys Res 111:D10107

Kumagai T, Mudd RG, Miyazawa Y, Liu W, Giambelluca TW, Kobayashi N, Lim TK, . . ., Yin S (2013) Simulation of canopy CO_2/H_2O fluxes for a rubber (*Hevea brasiliensis*) plantation in central Cambodia: the effect of the regular spacing of planted trees. Ecol Model 265:124–135

Lai C-T, Katul G, Oren R, Ellsworth D, Schäfer K (2000) Modelling CO_2 and water vapor turbulent flux distributions within a forest canopy. J Geophys Res 105:26333–26351

Lee X-H (1998) On meteorological observations of surface-air exchange over tall vegetation. Agric For Meteorol 91:39–49

Lee X-H, Finnigan J, Paw UKT (2004) Coordinate systems and flux bias error. In: Lee X-H, Massman W, Law B (eds) Handbook of Micrometeorology, A Guide for Surface Flux Measurement and Analysis. Kluwer Academic Publishers, Dordrecht, pp 33–66

Leuning R (2007) The correct form of the Webb, Pearman and Leuning equation for eddy fluxes of trace gases in steady and non-steady state, horizontally homogeneous flows. Bound Layer Meteorol 123:263–267

Lloyd CR (1995) The effect of heterogeneous terrain on micrometeorological flux measurements: a case study from HAPEX-SAHEL. Agric For Meteorol 73:209–216

Manzoni S, Katul G, Fay PA, Polley HW, Porporato A (2011) Modeling the vegetation-atmosphere carbon dioxide and water vapor interactions along a controlled CO_2 gradient. Ecol Model 222:653–665

Moncrieff JB, Jarvis PG, Valentini R (2000) Canopy fluxes. In: Sala OE, Jackson RB, Mooney HA, Howarth RW (eds) Methods in Ecosystem Science. Springer, New York, pp 161–180

Niinements U, Tenhunen JD (1997) A model separating leaf structural and physiological effects on carbon gain along light gradients for the shade-tolerant species *Acer sccharum*. Plant Cell Environ 20:845–866

Ohtsuka T, Saigusa N, Imura Y, Muraoka H, Koizumi H (2016) Biometric-based estimations of net primary production (NPP) in forest ecosystems. In: Hikosaka K, Niinemets Ü, Anten N (eds) Canopy Photosynthesis: From Basics to Applications. Springer, Berlin, pp 333–351

Raupach MR (1988) Canopy transport processes. In: Steffen WL, Denmead OT (eds) Flow and Transport in the Natural Environment. Springer, New York, pp 95–127

Schuepp PH, Leclerc MY, Macpherson JI, Desjardins RL (1990) Footprint prediction of scalar fluxes from analytical solutions of the diffusion equation. Bound Layer Meteorol 50:355–373

Stull RB (1988) An Introduction to Boundary Layer Meteorology. Kluwer Academic Publishers, Dordrecht

von Caemmerer S, Farquhar GD (1981) Some relationships between the biochemistry of photosynthesis and the gas exchange of leaves. Planta 153:376–387

Watanabe T (1993) The bulk transfer coefficients over a vegetated surface based on K-theory and 2nd-order closure model. J Meteor Soc Jpn 71:33–42

Webb EK, Pearman GI, Leuning R (1980) Correction of flux measurements for density effects due to heat and water vapour transfer. Quart J R Meteorol Soc 106:85–100

Wilson NR, Shaw RH (1977) A higher order closure model for canopy flow. J Appl Meteorol 16:1198–1205

Wilson KB, Baldocchi DD, Hanson PJ (2001) Leaf age affects the seasonal pattern of photosynthetic capacity and net ecosystem exchange of carbon in a deciduous forest. Plant Cell Environ 24:571–583